IEEE Access
Multidisciplinary | Rapid Review | Open Access Journal

Received August 26, 2020, accepted September 15, 2020, date of publication September 18, 2020,
date of current version September 30, 2020.

Digital Object Identifier 10.1109/ACCESS.2020.3024773

Reduction of the Induced Voltage in the Synchronous Generator Shaft Using Active AC / DC Converter

MOHAMAD ROSTAMI ENGASI[1], MAHMOUD SAMIEI MOGHADDAM[1], AND AMIN HAJIZADEH[2], (Senior Member, IEEE)

[1]Department of Electrical Engineering, Damghan Branch, Islamic Azad University, Damghan 19585-46655, Iran
[2]Department of Energy Technology, Aalborg University, 6700 Esbjerg, Denmark

Corresponding author: Mahmoud Samiei Moghaddam (samiei352@yahoo.com)

This work was supported by the University of Aalborg.

ABSTRACT Today, synchronous generators are broadly employed in the industry. The thyristor rectifier in the static excitation system of synchronous generators is responsible for supplying the DC voltage of the excitation winding. In these rectifiers, a high-frequency component is generated at the output of the DC voltage, during turning on and off of the thyristor. These high-frequency components charge the generator's parasitic capacitors. The voltage induced in these capacitors induces the voltage in the synchronous generator shaft. In this paper, the induced voltage analysis in the generator shaft is performed. Then, modeling, simulation, and experimental laboratory results of pulse width modulation are performed in the static generator excitation system. The induced voltage of the generator shaft is examined by applying this rectifier and it is compared and analyzed with the results of the thyristor rectifier. The hiring of a pulse width modulation rectifier has had a great impact on reducing the induced shaft voltage.

INDEX TERMS Shaft voltage, synchronous generator, rectifier, static excitation system.

NOMENCLATURE

$\mathcal{E}_0$	permittivity of a vacuum
$\mathcal{E}_R$	relative permittivity of the dielectric
R_B	bullet radius
R_C	clearance radius
N_B	bullet number
C_B	bearing capacitance
C_{SF}	capacitance between stator winding and body
Ns	number of stator slots
L_S, W_D W_S	lengths, width and height of the stator slot
D	dielectric constant
g	air gap
K_{RF}	constant coefficient of the stator to the rotor
R_S	inner radius of the stator
R_R	outer radius of the rotor
C_{RF}	capacitance between the rotor and the body
C_{RSH}	capacitance between the rotor and the shaft
C_{FW}	capacitance between the stator winding and the body
C_{WSH}	capacitance between the stator winding and the shaft
C_{FSH}	capacitance between the body and shaft
C_{0S}	capacitance between the body and stator
K_{SF}	constant coefficient of the stator winding to the body
K_{SR}	constant coefficient of the stator to the rotor
N_R	number of parallel conductors of the rotor
W_R, L_R	Width and length of the rotor
C	filter capacitor
R_C	internal resistance of filter capacitor
R_t	resistance of transistor
R_D	diode resistance
Ls, Lr	stator and rotor inductance
R_L	internal resistance of inductance
T_S	switching period

The associate editor coordinating the review of this manuscript and approving it for publication was Yue Zhang.

I. INTRODUCTION

Shaft voltages are among the phenomena that exist in rotating machines, and different sources contribute to the generation of these voltages. Shaft voltages result in currents to pass through the bearing. These destructive currents pass through the bearings oil and, over time, make some bubbles in

the oil, causing the bearings to fail. In some machines, especially when the impedance created by the shaft, bearing and frame is minimal, then large currents pass through this small impedance and cause significant damage to the bearing. Four sources for generating shaft voltage exist in rotary machines [1]. Therefore, it is essential to examine each of these sources separately for better and faster detection. These four factors are:

1. Magnetic asymmetry
2. Electromagnetic sources
3. Electrostatic sources
4. External voltage sources applied to the rotor windings

The small values of the shaft voltages are related to the electromagnetic induction caused by the electromagnetic sources and the magnetic asymmetry of the synchronous generators. A large amount of shaft induction voltage is because of the switching of power electronics devices in electric motor inverters and rectifiers of the excitation system of static synchronous generator. Magnetic asymmetry, electromagnetic sources, electrostatic sources, and external voltage sources applied to the rotor winding are four sources of shaft voltage generation in rotating machines. In [2] a passive filter at the PWM inverter output is designed to reduce the common mode and differential mode voltage created by the inverter. The use of the buck converter to decrease the induction voltage of the synchronous generator shaft has been carried out in [3]. Using an EMI Filter, [4], [5] have reduced bearing and ground leakage currents of a PWM diode clamp inverter. In [6] a common mode passive filter is used to decrease the motor shaft voltage and the induction motor bearing current fed by a two-level inverter. An EMI filter in [7] is designed for a PWM inverter consisting of two passive filters. These filters are incorporated into the inverter and motor outputs to compensate for the common-mode voltage resulted from the inverter, the neutral point of the motor and the rectifier. A hybrid EMI filter for compensation of common-mode inverter voltage is presented in [8]. The utilized low-frequency capacitor and series LC filter have been able to decrease the common-mode voltage. [9] shows that the common-mode voltage at the output of voltage source inverters (VSIs) causes an unwanted current in the bearings. Then, using an electrostatic circuit, some actions to decrease the common-mode voltage at the motor and rotor terminals have been performed. Some important works have been done to recognize the reasons of the shaft voltage and bearing current phenomenon. The static excitation system plays an essential role in the design of synchronous machines [10]. In [11] a 15-kW induction motor is driven using a PWM inverter and generates shaft voltage. The experimental results have shown that the parasitic capacitors with the high-frequency voltage of common-mode inside the motor, which has been created by the PWM inverter, are the cause of the shaft voltage. A new type of inverter is investigated in [12], results show that one of the bearings is subjected to induction current. The experimental results show that the measured currents and physical relationships of the proposed technique can validate the voltage reduction. A pulse-width modulation method is described in [13] for two- and three-level AC-DC-AC converters to decrease the common-mode voltage of these types of inverters in squirrel cage DFIGs. In [14], a method is proposed to calculate the impact of bearing insulation thickness to reduce its current as a function of machine design parameters. Reference [15] shows test results on the shaft voltage and bearing current of high voltage drivers that work with PWM. It is stated that PWM VSIs are the cause of bearing currents. Reference [2] Displays a new passive filter installed at the output of the PWM inverter terminals. This filter is used to eliminate the common mode and differential mode voltage created by the PWM inverter. In [16], a systematic analysis of common-mode voltage in different topologies of converters exploited in two-level AC drivers of VSIs, current source inverters, and multilevel inverters is described. The authors in [17] have discussed the shaft voltage created by a PWM inverter.

An equivalent circuit of the common mode of induction motor is given in [18]. They have expressed the effect of decreasing the shaft voltage by a new method. Exploiting the calculated shaft voltage from the equivalent circuit and the measured shaft voltage of the motor, they were able to confirm the validity of their method. Reference [19] provides a practical way to find a high-frequency model to predict the leakage current and shaft voltage of the AC machines. The impact of neutral point and rotor winding voltages on shaft voltage is studied in [20].

Details on four types of shaft voltages are given, with emphasis on the occurrence, transmission and damaging mechanisms of shaft voltages from static excitation systems is presented in [21]. A model for numerical simulation is presented, and simulation results are compared with tests performed on a statically excited 1200 MVA turbo Gen set. Moreover, in [1] This undesirable voltage affects the insulations gradually, lowering the life expectancy of the whole system. If the shaft voltage exceeds the dielectric breakdown voltage level of the lubricating grease film in journal bearings, an electrical discharge current flows through the bearings. A passive filter is proposed to overcome the stated issue to inspect the shaft voltage.

A nonmathematical description of the finite element analysis method is presented [22]. The application of the method to determining the excitation requirement of a large turbine generator is discussed. The handling of short-circuit behavior and end-region fields is considered. An extension of the finite element technique is described that allows one to find the electromagnetic fields, the winding currents, and the rotor motion simultaneously to understand the effect of harmonic current and voltage on large squirrel-cage induction motors. In [23] it gives a method to put into practice the FE method to analyses and design and electrical machines and apparatus.

In this paper, a new method by considering all the parasitic capacitors of the synchronous generator is presented for calculating the shaft voltage. A PWM rectifier has been used in the excitation system of the static synchronous generator,

to reduce the inductive voltage of the shaft against the thyristor rectifier. The PWM rectifier is intended as an active filter. This article considers the external voltage sources of the rotor winding as one of the fundamental reasons of the shaft voltage.

First, the parasitic generator capacitors are calculated by the FEM method with MAXWELL software. Then, the static excitation system is simulated with MATLAB software. The simulation and experimental results of the PWM rectifier are presented in the article to confirm the validation of the offered approach. In the second section of this paper, the suggested system modeling is presented. Then, in the third section, the simulation results are presented. Section 4 presents the experimental results of a static excitation system with a PWM rectifier. A conclusion is shown in the last section.

II. MODELING OF EXCITATION SYSTEM OF STATIC SYNCHRONOUS GENERATOR

The structure of the excitation system of the static synchronous generator is shown in Fig. 1. This structure includes a synchronous generator, PWM rectifier, and excitation transformer. The generator bearings connection to the body has been insulated by polyamide to make it possible to measure the generator shaft voltage. The three-phase AC voltage is applied to the PWM rectifier by the excitation transformer and at the rectifier output, the required DC voltage for the excitation system of synchronous generator Winding is provided.

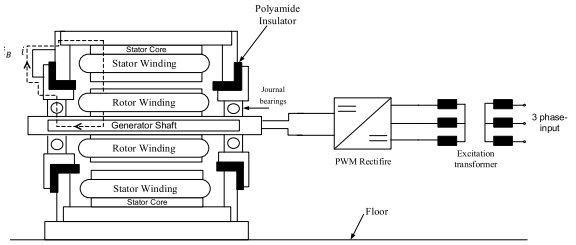

FIGURE 1. Structure of the static excitation system of synchronous Generator with PWM rectifier.

The finite element method (FEM) is used to compute the parasitic capacitances. Maxwell software hires the precise.

FEM to solve static, frequency-domain, and time-variant electromagnetic. To make a better overview and explain properly the connections of parasitic capacitors, the synchronous generator is divided into 6 separate parts (nodes) including the stator, stator winding, rotor, shaft, field winding, and frame. Figure 2 displays these parts equivalent to the electrical arrangement. Moreover, all the parasitic capacitors with separate parts in synchronous generator are presented in detailed connection Figure 3.

A. CALCULATION OF PARASITIC CAPACITORS

In this section, the parasitic capacitors of a 5 kW synchronous generator are obtained using numerical modeling [24], [25]. The bearing capacitance is related to the geometrical structure

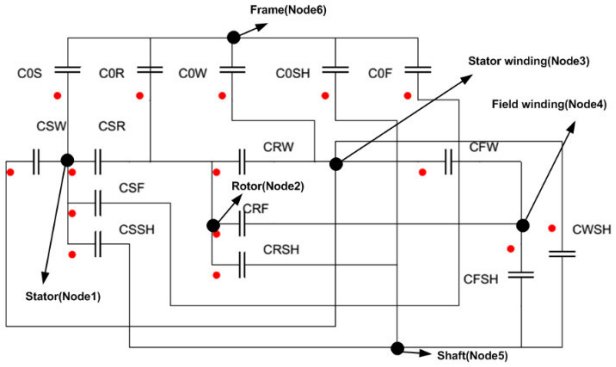

FIGURE 2. Six different parts of the synchronous generator used to calculate the parasitic capacitances.

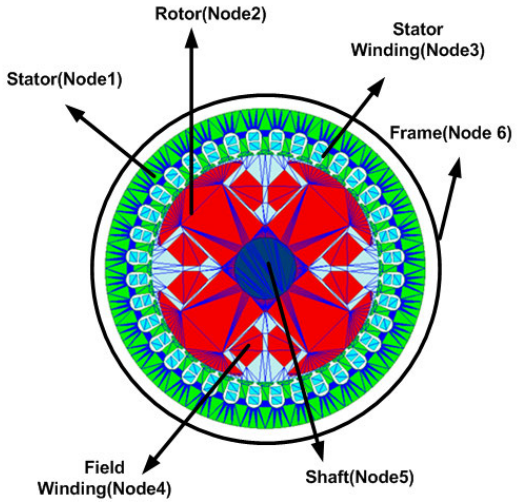

FIGURE 3. Detailed connection of parasitic capacitances.

of the bearing, load, speed, temperature, and characteristics of the lubricant.

$$C_b = \frac{N_b 4\pi \varepsilon_0 \varepsilon_r}{(\frac{1}{R_b} - \frac{1}{R_b+R_c})} \quad (1)$$

In equation (1), N_b is the number of bearings shot, R_b is the shot radius, and R_c is the clearance radius. To calculate this capacitor, the dielectric coefficient used in the bearing must be obtained. In this generator, grease is used in the bearings. Equation (1) is used to obtain the capacitor of the bearing. Bearing capacitors depend on the geometric structure of the bearing, load, speed, heat and oil properties [26].

$$C_{sf} = \frac{K_{sf} N_s \varepsilon_r \varepsilon_0 (W_{d+} W_s) L_s}{d} \quad (2)$$

Equation (2) is used to calculate the capacitor between the stator winding and the body [1].

N_s are the number of stator slots and L_s, W_d, and W_s are the lengths, width, and height of the stator slot, respectively. d is the stator winding dielectric. The parameters ε_0 and ε_r are the permeability coefficients of the vacuum and the dielectric in

the stator winding. K_{sf} is the constant coefficient of the stator winding to the body.

The stray capacitor between the stator and rotor is calculated according to (3) [27].

$$C_{sr} = \frac{K_{sr} N_r \varepsilon_0 W_r L_r}{g} \tag{3}$$

In this equation, N_r is the number of parallel conductors of the rotor. L_r is the length of the rotor, and W_r is the width of the rotor. The parameter g is the distance between the stator and the rotor, and Ksr is the constant coefficient of the stator to the rotor. Equation (4) shows the calculation capacitance between the rotor and the body [27].

$$C_{rf} = \frac{K_{rf} \pi \varepsilon_0 L_r}{\ln(\frac{R_s}{R_r})} \tag{4}$$

In this equation, Rs is the inner radius of the stator and R is the outer radius of the rotor. The K_{rf} is the constant coefficient of the rotor to the body. Fig. 4 shows an investigation procedure of the synchronous generator parasitic capacitor's dimensions.

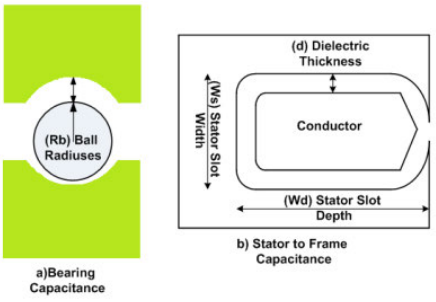

FIGURE 4. The structure of some parts of the synchronous generator for calculating parasitic capacitors.

B. MODELING PWM RECTIFIER

Recently, PWM rectifiers have been exploited in various applications. Due to less voltage stress and a more comprehensive range of output voltage, buck rectifiers have advantages over boost rectifiers in high power applications. This section discusses the type of buck rectifier that uses an input LC filter. The filter is used to eliminate high-frequency switching peaks. Furthermore, this results in the unwanted phase shift and the power factor deterioration. The phase shift is highly dependent on the modulation index and the phase angle of the PWM algorithm. This is because of the sophisticated control of this rectifier. Different control methods have been proposed for the PWM buck rectifier. However, they are mostly founded on simple models that merely consider steady-state, ignore input filter properties, or use single-phase models. Since the dynamics of the actual converters change with the change of working point, it is clear that the application of such simple models does not provide a perfect model and good rectifier stability [28], [29]. This article discusses the complete model of the PWM buck rectifier. Accurate linear equivalent circuits are employed for both DC and AC sides for static and dynamic analysis.

1) DQ TRANSFORMATION

The PWM buck rectifier is illustrated in Fig. 5. Because of switching, this system can be considered as a time-varying system. However, the other elements are LTI.

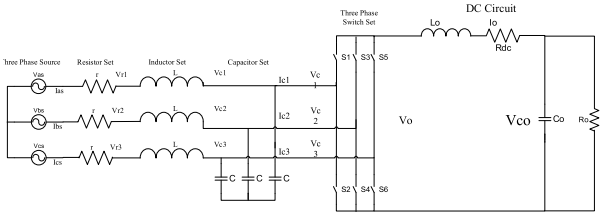

FIGURE 5. Structure of the PWM rectifier.

This makes it impossible to use conventional LTI analysis. However, the DQ transformation makes it possible to use circuit analysis. For this purpose, the following three steps should be taken:

A) The circuit is divided into basic sub-circuits.

B) Each sub-circuit is transformed to dq circuits based on equations. This eliminates the time-varying nature of the switching system. The three-phase balanced voltage switching sources, dq transformation matrix, and the related equations are brought below.

C) The transformed sub-circuits can be connected to adjacent nodes to form the complete circuit [28].

$$V_{abc} = \begin{bmatrix} v_{as} \\ v_{bs} \\ v_{cs} \end{bmatrix} = V_s. \begin{bmatrix} \sin(\omega t + \varphi_1) \\ \sin(\omega t - 2\pi/3 + \varphi_1) \\ \sin(\omega t + 2\pi/3 + \varphi_1) \end{bmatrix} \tag{5}$$

$$S_{abc} = \begin{bmatrix} s_a \\ s_b \\ s_c \end{bmatrix} = m. \begin{bmatrix} \sin(\omega t + \varphi_2) \\ \sin(\omega t - 2\pi/3 + \varphi_2) \\ \sin(\omega t + 2\pi/3 + \varphi_2) \end{bmatrix} \tag{6}$$

$$V_{dq0} = \begin{bmatrix} v_q v_d v_0 \end{bmatrix}' = K.V_{abc}, V_{abc} = K^{-1}.V_{qd0} \tag{7}$$

$$V_{dq0} = \begin{bmatrix} v_q v_d v_0 \end{bmatrix}' = K.V_{abc}, V_{abc} = K^{-1}.V_{qd0} \tag{8}$$

In this rectifier, the switches are assumed to be ideal. Therefore, based on the above equations, this circuit is divided into six basic sub-circuits, according to Fig. 6. The LTI equivalent circuit of the rectifier is illustrated in Fig. 7.

Since φ in the *dq* transformation of k in (8) can be chosen independent of system performance, without loss of the generality of problem, the obtained equivalent circuit can be simplified by choosing φ and $\varphi 2$, according to Fig. 7. The circuit in Fig. 3 shows the entire dynamic properties of the rectifier. Therefore, it can be exploited for dynamic simulation.

According to Fig. 7, the order of the system is decreased to six and the stability of the system, as long as the passive circuit elements are kept constant, only changes with the modulation index (m). It should be mentioned that the power angle ($\theta = \varphi_1 - \varphi_2$) does not alter the poles of the system

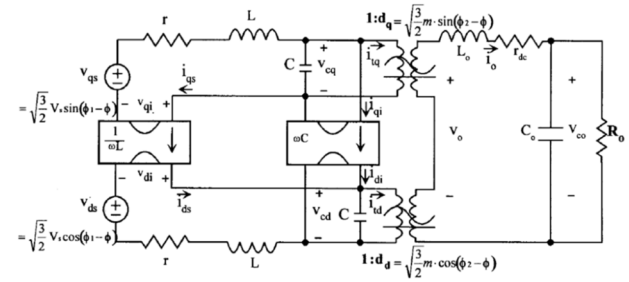

FIGURE 6. The equivalent circuit of the rectifier in dq frame.

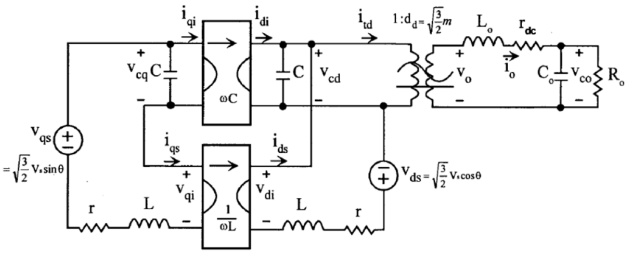

FIGURE 7. The simplified dq equivalent circuit.

but alters the zeros of the system. These specifications can be obtained by analyzing the equations.

C. STEADY-STATE ANALYSIS

DC equivalent circuit, which shows the steady-state characteristics of the converter, can be attained by considering the inductors short-circuited and contemplating the capacitors open-circuited (see Fig. 8). In the DC circuit, the momentary circuit variables and the variable parameters (i, v, m, θ, ω) are the static variables. The electrical DC variables are shown in capital letters. We will also show steady-state parameters by adding an index (0). The AC side resistance of the inductor is omitted in the DC analysis because its value is too small and makes the analysis very simple.

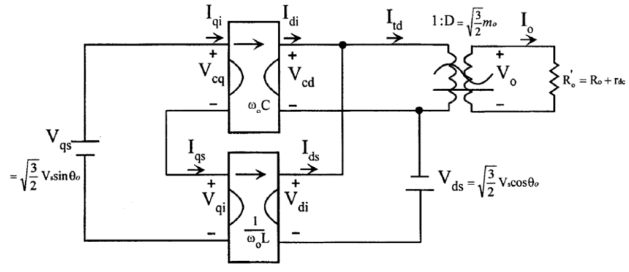

FIGURE 8. DC equivalent circuit of the rectifier.

Since the input currents of the two gyrators are constant, it can be stated that [1]:

$$I_{qi} = \omega_0 C V_{cd} = I_{qs} = \frac{(V_{cd} - V_{ds})}{\omega_0 L} \tag{9}$$

$$V_{cd} = \frac{V_{ds}}{1 - \omega_0^2 LC} V_s \tag{10}$$

$$V_0 = DV_{cd} = \frac{3}{2} \times \frac{m_{0cos\theta_0}}{1 - \omega_0^2 LC} V_s \tag{11}$$

$$(V_{cq} = \sqrt{\frac{3}{2}} \frac{V_s}{1 - \omega_0^2 LC} \left(sin\theta_0 - \frac{3}{2} \times \frac{\omega_0 L m_0 2cos\theta_0}{\left(1 - \omega_0^2 LC\right) \grave{R}_0} \right) \tag{12}$$

$$I_{ds} = \frac{V_{cq}}{\omega_0 L} = \sqrt{\frac{3}{2}} \times \frac{V_s}{1 - \omega_0^2 LC} \times \left(\frac{3}{2} \times \frac{m_0 2cos\theta_0}{\left(1 - \omega_0^2 LC\right) \grave{R}_0} - \omega_0 C sin\theta_0 \right) \tag{13}$$

$$I_{qs} = \omega_0 C V_{cd} = \sqrt{\frac{3}{2}} \times \frac{\omega_0 C cos\theta}{\left(1 - \omega_0^2 LC\right)} V_s \tag{14}$$

From (11), it is clear that the output voltage is not dependent to load resistance. This shows that the output voltage of the converter can be considered as an ideal voltage source controlled by θ_0 and m_0. Moreover, the DC gain varies from zero to a maximum. If the resonance frequency of the AC side LC filter is set close to ω_0, this gain can be much greater than one. However, in a real system, this gain is constrained to a certain value where the filter resonance frequency is much greater than the line frequency, which results in a slight increment in the DC gain. The switching function parameters such as θ_0 and m_0, are able to control the gain. The power of the AC source is calculated as follows [1]:

$$P = V_{qs} I_{qs} + V_{ds} I_{ds} = \frac{3}{2} \frac{V_s^2 . cos^2\theta_0}{1 - \omega_0^2 LC} . Y \tag{15}$$

$$Y = \frac{3}{2} \frac{m_0^2 .}{1 - \omega_0^2 LC} \frac{1}{R_0} \tag{16}$$

The reactive power is calculated as follows:

$$Q = V_{qs} I_{ds} - V_{ds} I_{qs} \frac{V_s^2}{1 - \omega_0^2 LC} . (Ycos\theta_0 sin\theta_0 - \omega_0 C) \tag{17}$$

The first part of (17) shows the variable reactive power created by the converter that can be controlled by θ_0. This indicates that while m_0 is predetermined for specified output power, the reactive power, either leading or lagging, can only be controlled by the phase difference of θ_0. The second part means that the maximum fixed reactive power is created by the input AC filter. Therefore, the converter produces the same amount of lagging reactive power. Active and reactive power is normalized by the coefficient $\frac{V_s^2}{R_0}$. The power factor is calculated as follows [1]:

$$PF = \frac{P}{\sqrt{P^2 + Q^2}} = \frac{cos^2\theta_0}{\sqrt{\left(\frac{\omega_0 C}{Y}\right)^2 - \left(\frac{\omega_0 C}{Y}\right) sin2\theta_0 + cos^2\theta_0}} \tag{18}$$

From (17), the unity power factor conditions can be obtained as follows [1]:

$$Ycos\theta_0 sin\theta_0 \omega_0 C = 0 \tag{19}$$

$$\theta_0 = \frac{1}{2} sin^{-1}(\omega_0 C/Y) \quad for\ Y \geq 2\omega_0 C \tag{20}$$

While (Y) is less than $2\omega_0$C the power factor cannot be equal to one. This occurs when the high resistance load. The power factor can be controlled as a function of the control variables 0 and m0. Although there are two points for the coefficient, only one of them is between 0 and 45 degrees that it can be exploited in practice to obtain the output voltage. In this area, the rectifier is able to supply maximum power with high power factor but in the range of 45 to 90 degrees, the power factor varies with phase change and the power gain is low. Under the unity power factor, according to (18), the converter has significant properties. As an instance, the output current of the inductor is obtained from the following relation [1]:

$$I_0 = \frac{3}{2} \frac{V_s cos\theta_0}{1 - \omega_0^2 LC} \frac{m_0}{R'_0} \tag{21}$$

It should be mentioned that while the power factor is equal to one, the DC side voltage and the active power and current could only be controlled by the modulation index, which is not dependent on phasing difference. Operating in all ranges is useful and essential for rectifier design and control. The alteration of gain, reactive power, active power, and power factor due to changes in the working point was shown. While the phase difference tends to zero, the actual gain and power increase, but it has to lead reactive power at $-45°$ and maximum lagging reactive power at 45°. Internal resistance changes the range of electrical quantities, but these changes are not significant.

D. THE SIMPLIFIED DYNAMIC CHARACTERISTICS

Previous precise AC models are acceptable, but from an engineering point of view, in practice, these models are very complicated. Therefore, the development of a simplified model is essential for practical purposes. The converter has two main properties: first, the fast response; second, the AC filter response at the DC side is slow. These two parts are coupled to each other via a rectifier switch. If the control objectives are power factor correction and output voltage and current regulation, a slow response circuit is preferred to a fast response circuit. In this respect, AC-side circuits are considered as ideal voltage sources at a specified operating point, and the immediate response characteristics are ignored. Therefore, a simplified model is attained in which the AC side filters are considered at a steady-state while the DC side filters are considered at transient state. Three distorted voltage sources exist:

$$\widehat{v_\theta}(s) = -\sqrt{\frac{3}{2}} \frac{V_s sin\theta_0}{1 - \omega_0^2 LC} \hat{\theta}(s) \tag{22}$$

$$\widehat{v_\theta}(s) = -\frac{3}{2} \frac{V_s cos\theta_0}{1 - \omega_0^2 LC} \hat{m}(s) \tag{23}$$

$$\widehat{v_\theta}(s) = \sqrt{\frac{3}{2}} \frac{V_s cos\theta_0}{1 - \omega_0^2 LC} \hat{v_s}(s) \tag{24}$$

Since this model contains complete data about AC input filters and working point current, the simplified model is different from the simplified output model in which the input properties are ignored. The preciseness of this simplified model is recognized by the degree of separation between AC filter poles and DC filter poles. This simplified AC model is very fruitful for fast controller design.

The values in Table 1 are PWM rectifier parameters.

TABLE 1. The PWM rectifier parameters.

Parameters	values
L (Inductance)	530 μH
R_L (Inductance resistance)	25 $m\Omega$
C (Capacitor)	570 μF
R_C (resistance of capacitor)	65 $m\Omega$
R_t (resistance in the transistor)	20 $m\Omega$
$_D$ (diode resistor)	25 $m\Omega$
V_g (input voltage)	45 V
V_o (output voltage)	30 V
T_s (switching period)	25μs

III. SIMULATION RESULTS FOR EXCITATION SYSTEM WITH PWM RECTIFIER

Fig. 9 presents a schematic of the static excitation system of the synchronous generator considering a PWM rectifier. This rectifier converts AC voltage to required DC voltage of generator excitation winding.

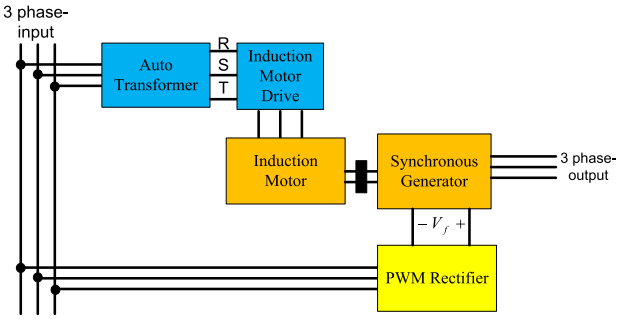

FIGURE 9. The schematic diagram of the simulated system with a PWM rectifier.

Before presenting the simulation results, the parasitic capacitor values from the MAXWELL software are given in Table 2.

TABLE 2. The parasitic capacitor values from the MAXWELL software.

Capacitance	Parasitic capacitance (PF)
C_{SW}	8207.3
C_{SR}	3480.7
C_{SSH}	2319.3
C_{SF}	1035.3
C_{0R}	333.26
C_{0S}	367.74
C_{0W}	352.33
C_{0F}	273.51
C_{0SH}	332.68
C_{RW}	2449
C_{RF}	1418.2
C_{RSH}	758.09
C_{FW}	918.18
C_{WSH}	2446.6
C_{FSH}	1418.1

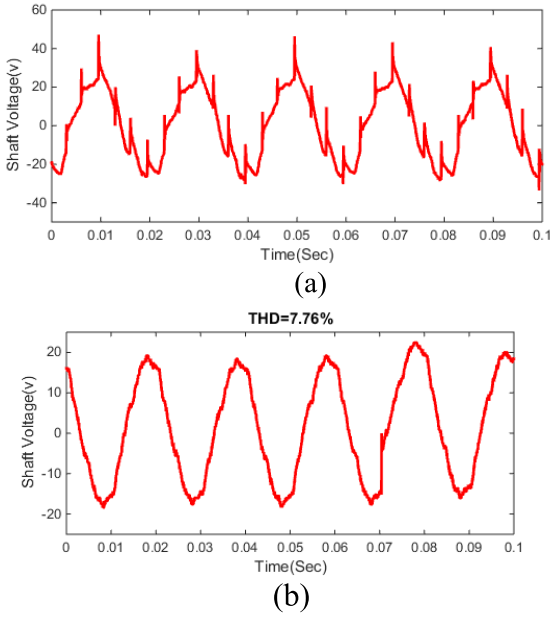

FIGURE 10. Simulation results of the shaft voltage a) without filter b) with PWM rectifier.

By simulating the proposed static excitation system model, the shaft voltage can be obtained with and without the PWM rectifier. The synchronous generator shaft voltage is illustrated in Fig. 11.

The simulation results when a PWM rectifier is used in the static excitation system of the synchronous generator are shown. Since a passive LC filter is used in the buck converter structure, the system dynamics are slow, and the AVR system response is slowed down, which is one of the significant disadvantages of this regulator. However, using a PWM rectifier and by applying a high cut-off frequency, the components of the passive filter have become smaller, and the response of the static excitation system is faster in response to the input voltage changes. This rapid response is shown in the simulation results. In the experimental results,

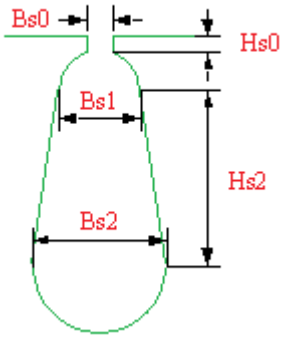

FIGURE 11. Synchronous generator stator groove.

which are brought in the next section, it is demonstrated that the experimental results confirm the simulation results.

Table 3 shows the values of the shaft voltages and their THD values. The value of the shaft voltage range reaches 80.4 V when the filter is not applied to the rectifier output. The shaft voltage is reduced to 3.9 V by applying a PWM rectifier. By applying the PWM rectifier in a static excitation system, a 95.1% reduction in the shaft induction voltage is observed. Table 4 shows the technical specifications and dimensions of the generator according to the measurements taken.

TABLE 3. Comparison of shaft voltage in different conditions.

PWM rectifier	Without filter	Measured parameter
3.9v	80.4v	Shaft voltage amplitude
7.76%	19.03%	Shaft voltage THD

TABLE 4. Synchronous generator dimensions and specifications.

External stator diameter	251 mm	Internal stator diameter	179mm	Engine length	103.4 mm
air gap	0.5 mm	External diameter of rotor	178mm	Nominal voltage	380v
External diameter of the rotor	178 mm	Stainless Steel Material	Stainless Steel 1010	Internal rotor diameter	48.4 mm
Winding step	3	Stator Groove Number	36	Number of poles	4
Pole shaft width	92 mm	Number of conductors per groove	42	Type of wiring distributed layer	2
Groove opening	2.87 mm	Nominal speed	1800 rpm	output power	5kw

Moreover, the synchronous generator stator groove is presented in Fig.11.

According to Fig.11, all parameters are given in Table 5.

TABLE 5. The parameters of synchronous generator stator groove.

Parameters	values
Hs_0	$1.42mm$
Hs_2	$11mm$
Bs_0	$2.87mm$
Bs_1	$9.7mm$
Bs_2	$12.8mm$

IV. THE MEASURED VOLTAGES BY EMPLOYING PWM RECTIFIER

Fig. 12 shows an overview of the equipment made in the laboratory. This equipment includes a driver, a 5 kW synchronous generator, and a PWM rectifier.

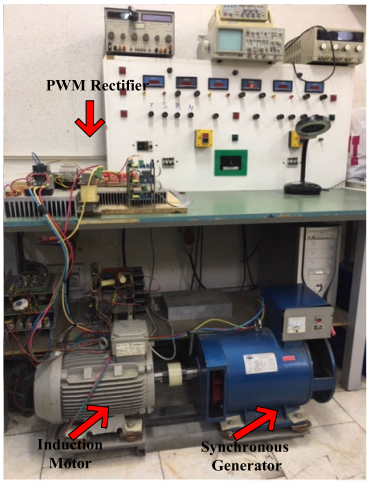

FIGURE 12. The prototype system of a synchronous generator with PWM rectifier.

The input voltage of the synchronous generator excitation winding is shown in Fig. 13 a under the no-filter condition and the condition in which the PWM rectifier is employed. Obviously, according to Fig. 13 b, the amplitude of the high-frequency components of the PWM rectifier has reached the minimum value by using the PWM rectifier. Precisely, 96% reduction is achieved in this condition.

The reduced value of the high-frequency components of the excitation winding input voltage is shown for both without filter and with the PWM rectifier condition in the figure. The transient state voltage amplitude of the rectifier without the filter is 189 V. However, as expected, the amplitude of this voltage was reduced to 0.45 V by applying a PWM rectifier to the excitation winding. The reduced value indicates that 98% reduction has been achieved by using the regulator.

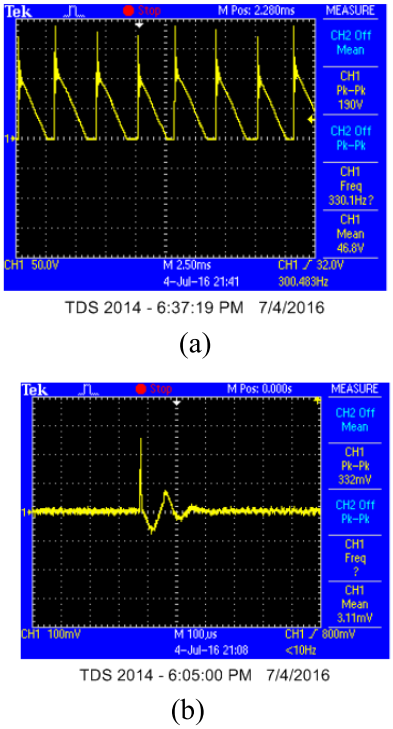

FIGURE 13. The excitation winding input voltage a) without filter b) with PWM rectifier.

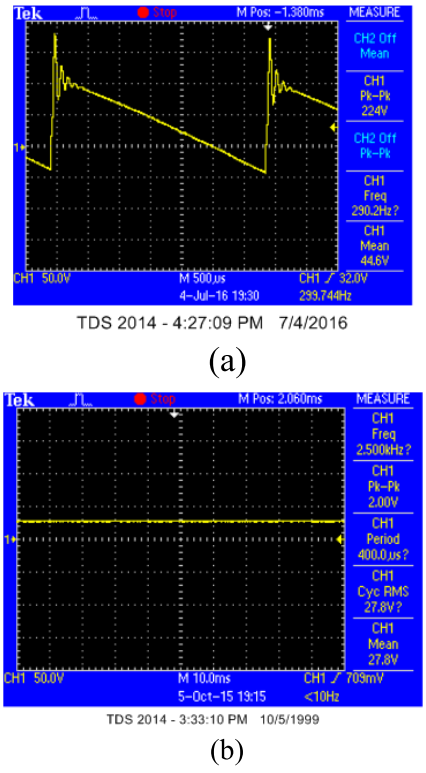

FIGURE 14. The amplitude of the high-frequency voltage of the shaft a) without filter b) with PWM rectifier.

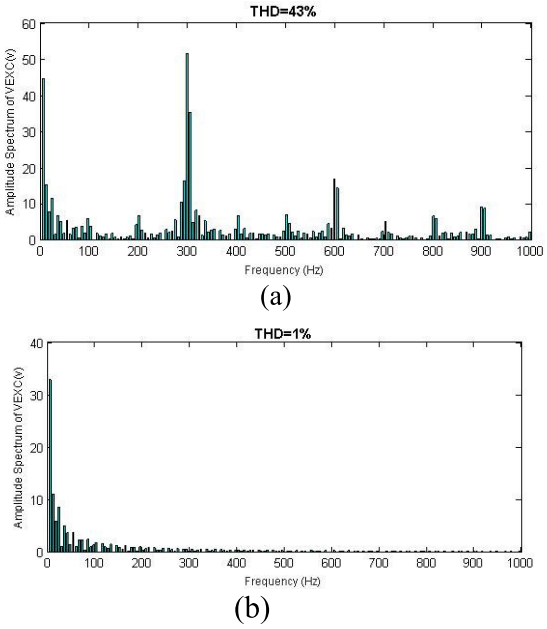

FIGURE 15. The frequency spectrum of the input voltage the excitation winding of the synchronous generator. a) Without filter. b) With a PWM rectifier.

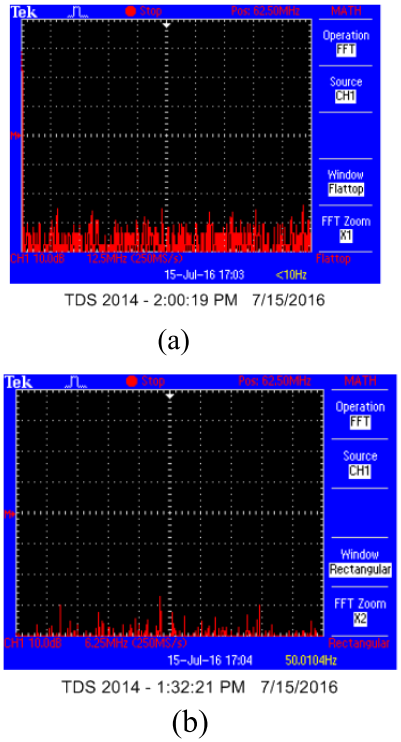

FIGURE 16. Fourier transformation of input voltage of the excitation winding a) without filter b) with PWM rectifier.

The high-frequency components of the shaft voltage are illustrated in Fig. 14 for the condition in which the rectifier output is directly connected to the excitation winding and the case. In this case, the voltage regulator is connected to the rectifier output. Moreover, the amplitude of the high-frequency

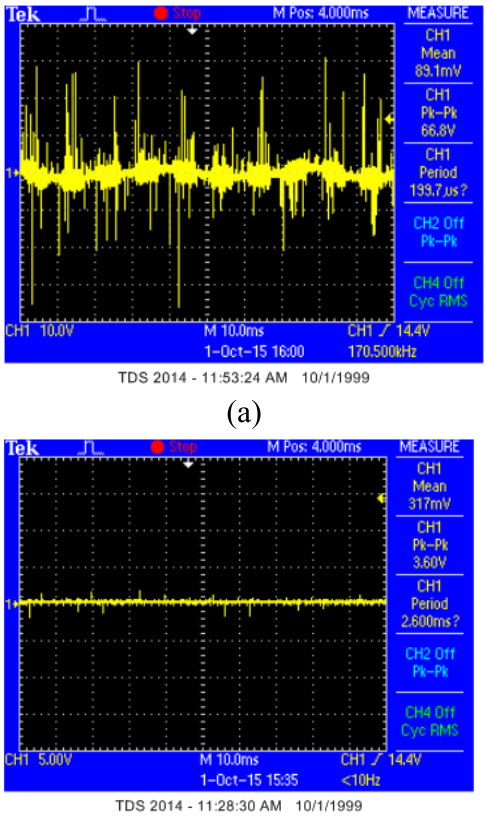

FIGURE 17. The synchronous generator shaft voltage a) without filter b) with PWM rectifier.

voltage of the shaft is 25.4V for the condition in which no filter is connected. The amplitude of the high-frequency component of this voltage is reduced to 0.34 V when a PWM rectifier is employed. As shown, it is much less than in the no-filter condition.

A. THE FREQUENCY SPECTRUM OF VOLTAGES OBTAINED WITH PWM RECTIFIER

Fig. 15shows the frequency spectrum of the experimental results for the input voltage of the excitation winding. The shaft induction voltage range depends on the rectifier's DC-side filters. Therefore, the higher the peak frequency of the synchronous generator winding, the impact of the parasitic capacitors is reduced, and the shaft induction voltage is reduced. The reduction of the high-frequency components of the input voltage of the excitation winding by the PWM rectifier has the highest value, indicating that the PWM rectifier played a crucial role in reducing the effect of the parasitic capacitors. The results validate the simulation results.

The Fourier transformation of the input voltage of the synchronous generator excitation winding, measured and calculated by the TDS2014 digital oscilloscope, is shown in Fig. 16. The high-frequency components of the excitation winding input voltage in the case in which a PWM rectifier is used in the static excitation system and a six-pulse

rectifier is directly connected to the generator excitation are illustrated in Fig. 16 (a). As shown in Fig. 16(b), after employing the PWM rectifier, these components have significantly decreased.

From the figure above, the PWM rectifier is able to reduce the amplitude of the high-frequency output voltage of the rectifier that means the influence of the parasitic capacitors in the synchronous generator has been decreased. This reduction results in the decrement of the induction voltage in the generator shaft.

The reduction of the shaft induction voltage is dependent on the rectifier's output filters. The spikes caused by the switching of the rectifier's thyristors cause high-frequency peaks. Using an active voltage regulator, these spikes can be converted to low amplitude ripples. Applying this DC voltage to the excitation winding with the least possible amplitude of the high-frequency components reduces the effect of the parasitic capacitors and the shaft induction voltage amplitude. As illustrated in Fig. 17 (a), the high-frequency peaks of the rectifier switching operation exist in the shaft voltage. Applying the PWM rectifier to the static excitation system, the maximum inductive voltage drop is obtained as shown in Fig. 17 (b). This PWM rectifier is able to reduce these high-frequency peaks to its least possible value.

V. CONCLUSION

In the static excitation system, the switching of thyristors leads to the creation of high-frequency peaks in the rectifier's DC output. These high-frequency peaks create the parasitic capacitors in the synchronous generator. When the path of the parasitic capacitors is closed through the generator shaft, a significant voltage is induced on the shaft. In this paper, first, the simulation of the PWM rectifier has been presented. Then, the simulation results for excitation winding input voltage, phase voltages and the synchronous generator shaft voltages with and without applying PWM rectifier are presented. Finally, the frequency spectrum of these voltages is discussed. The PWM rectifier is used to reduce the synchronous generator's shaft voltage. Adding a PWM rectifier to the excitation system, the amplitude of the high-frequency components has been reduced by up to 95% and the dynamics response of the excitation system is improved. The filters affect the reduction of shaft voltage, but the use of the PWM rectifier at the output stage of the excitation system has the most crucial impact. Reducing the generator shaft voltage leads to a longer lifetime of the synchronous generator bearings.

REFERENCES

[1] R. K. Golkhandan, M. Tavakoli Bina, M. A. Golkar, and M. Jokar, "A complete excitation-shaft-bearing model to overcome the shaft induced voltage and bearing current," in *Proc. 2nd Power Electron., Drive Syst. Technol. Conf.*, Feb. 2011, pp. 362–366.

[2] X. Dianguo, G. Qiang, and W. Wei, "Design of a passive filter to reduce common-mode and differential-mode voltage generated by voltage-source PWM inverter," in *Proc. 32nd Annu. Conf. IEEE Ind. Electron. IECON*, Nov. 2006, pp. 2483–2487.

[3] M. S. Moghaddam, M. T. Bina, M. A. Golkar, and S. S. Kojori, "Optimal design of voltage regulators for static excitation system in synchronous generator to reduce shaft-induced voltage," *TURKISH J. Electr. Eng. Comput. Sci.*, vol. 25, pp. 1827–1839, May 2017, doi: 10.3906/elk-1602-184.

[4] H. Akagi and S. Tamura, "A passive EMI filter for eliminating both bearing current and ground leakage current from an inverter-driven motor," *IEEE Trans. Power Electron.*, vol. 21, no. 5, pp. 1459–1469, Sep. 2006.

[5] H. Akagi and S. Tamura, "A passive EMI filter for eliminating both bearing current and ground leakage current from an inverter-driven motor," in *Proc. IEEE 36th Conf. Power Electron. Specialists*, Jun. 2005, pp. 2442–2450.

[6] J. Kalaiselvi and S. Srinivas, "Passive common mode filter for reducing shaft voltage, ground current, bearing current in dual two level inverter fed open end winding induction motor," in *Proc. Int. Conf. Optim. Electr. Electron. Equip. (OPTIM)*, May 2014, pp. 595–600.

[7] A. Esmaeli, "Mitigation of the adverse effects of PWM inverter through passive cancellation method," in *Proc. 1st Int. Symp. Syst. Control Aerosp. Astronaut.*, Jan. 2006, p. 5.

[8] P. Pairodamonchai, S. Suwankawin, and S. Sangwongwanich, "Design and implementation of a hybrid output EMI filter for high-frequency common-mode voltage compensation in PWM inverters," *IEEE Trans. Ind. Appl.*, vol. 45, no. 5, pp. 1647–1659, Sep./Oct. 2009.

[9] D. Hyypio, "Mitigation of bearing electro-erosion of inverter-fed motors through passive common-mode voltage suppression," *IEEE Trans. Ind. Appl.*, vol. 41, no. 2, pp. 576–583, Mar. 2005.

[10] A. K. Datta, M. Dubey, and S. Jain, "Modelling and simulation of static excitation system in synchronous machine operation and investigation of shaft voltage," *Adv. Electr. Eng.*, vol. 2014, pp. 1–9, Jul. 2014.

[11] U. T. Shami and H. Akagi, "Experimental discussions on a shaft end-to-end voltage appearing in an inverter-driven motor," *IEEE Trans. Power Electron.*, vol. 24, no. 6, pp. 1532–1540, Jun. 2009.

[12] A. Muetze, "On a new type of inverter-induced bearing current in large drives with one journal bearing," *IEEE Trans. Ind. Appl.*, vol. 46, no. 1, pp. 240–248, Nov. 2010.

[13] M. E. Adabi and A. Vahedi, "A survey of shaft voltage reduction strategies for induction generators in wind energy applications," *Renew. Energy*, vol. 50, pp. 177–187, Feb. 2013.

[14] A. Muetze and A. Binder, "Calculation of influence of insulated bearings and insulated inner bearing seats on circulating bearing currents in machines of inverter-based drive systems," *IEEE Trans. Ind. Appl.*, vol. 42, no. 4, pp. 965–972, Jul. 2006.

[15] F. Wang, "Motor shaft voltages and bearing currents and their reduction in multilevel medium-voltage PWM voltage-source-inverter drive applications," *IEEE Trans. Ind. Appl.*, vol. 36, no. 5, pp. 1336–1341, Sep. 2000.

[16] S. Wei, N. Zargari, B. Wu, and S. Rizzo, "Comparison and mitigation of common mode voltage in power converter topologies," in *Proc. Conf. Rec. IEEE Ind. Appl. Conf., 39th IAS Annu. Meeting.*, Oct. 2004, pp. 1852–1857.

[17] U. T. Shami and H. Akagi, "Identification and discussion of the origin of a shaft end-to-end voltage in an inverter-driven motor," *IEEE Trans. Power Electron.*, vol. 25, no. 6, pp. 1615–1625, Jun. 2010.

[18] U. T. Shami and H. Akagi, "Identification and Discussion of the origin of a shaft end-to-end voltage in an inverter-driven motor," *IEEE Trans. Power Electron.*, vol. 25, no. 6, pp. 1615–1625, Jun. 2010, doi: 10.1109/TPEL.2009.2039582.

[19] F. Zare, "Practical approach to model electric motors for electromagnetic interference and shaft voltage analysis," *IET Electr. Power Appl.*, vol. 4, no. 9, p. 727, 2010.

[20] J. Adabi, F. Zare, and A. Ghosh, "End-winding effect on shaft voltage in AC generators," in *Proc. 13th Eur. Conf. Power Electron. Appl.*, vol. 10, Sep. 2009, pp. 8–10.

[21] C. Ammann, K. Reichert, R. Joho, and Z. Posedel, "Shaft voltages in generators with static excitation systems-problems and solution," *IEEE Trans. Energy Convers.*, vol. 3, no. 2, pp. 409–419, Jun. 1988.

[22] S. J. Salon, *Finite Element Analysis of Electrical Machines*. Norwell, MA, USA: Kluwer, 1995.

[23] R. Bargallo, *Finite Element for Electrical Engineering*, 2th ed. Hoboken, NJ, USA: Wiley, 2006.

[24] W. H. Hayt, *Engineering Electromagnetics*, 5th ed. New York, NY, USA: McGraw-Hill, 1989.

[25] D. Busse, J. Erdman, R. J. Kerkman, D. Schlegel, and G. Skibinski, "System electrical parameters and their effects on bearing currents," *IEEE Trans. Ind. Appl.*, vol. 33, no. 2, pp. 577–584, Mar. 1997.

[26] W. H. Hayt, *Engineering Electromagnetics*, 5th ed. New York, NY, USA: McGraw-Hill, 1989.
[27] H.-R. Wang, G.-R. Zhu, D.-H. Zhang, W. Chen, and Y. Chen, "On the practical design of a single-stage single-switch isolated PFC regulator based on sliding mode control," in *Proc. 7th Int. Power Electron. Motion Control Conf.*, Jun. 2012, pp. 719–724.
[28] S.-B. Han, N.-S. Choi, C.-T. Rim, and G.-H. Cho, "Modeling and analysis of static and dynamic characteristics for buck-type three-phase PWM rectifier by circuit DQ transformation," *IEEE Trans. Power Electron.*, vol. 13, no. 2, pp. 323–336, Mar. 1998.
[29] H. Lei, E. Xiao, J. Xiong, X. Lin, and Y. Kang, "Modeling and analysis of three-phase four-leg PWM boost-type rectifier for double conversion transformerless UPS," in *Proc. 37th Annu. Conf. IEEE Ind. Electron. Soc. IECON*, Nov. 2011, pp. 1444–1449.

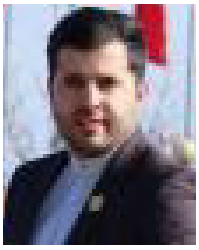

MOHAMAD ROSTAMI ENGASI received the master's degree from Islamic Azad University, Damghan Branch, in 2015, where he is currently pursuing the Ph.D. degree in electrical engineering.

MAHMOUD SAMIEI MOGHADDAM received the M.A. degree from Khaje Nasir University, in 2005, and the Ph.D. degree in electrical engineering from the K. N. Toosi University of Technology, Tehran, Iran, in 2016. Since 2005, he has been a Faculty Member of Islamic Azad University, Damghan Branch. He has published numerous articles in the field of power.

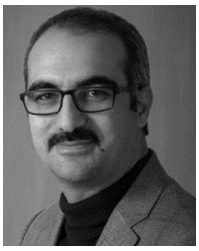

AMIN HAJIZADEH (Senior Member, IEEE) received the B.S. degree from Ferdowsi University, Mashad, Iran, in 2002, and the M.S. (Hons.) and Ph.D. (Hons.) degrees from the K. N. Toosi University of Technology, Tehran, Iran, in 2005 and 2010, respectively, all in electrical engineering. He held a postdoctoral position with the Norwegian University of Science and Technology, Trondheim, Norway, from 2015 to 2016. Since 2016, he has been an Associate Professor with the Department of Energy Technology, Aalborg University. His current research interests include control of distributed energy resources, design and control of power electronic converters for microgrid, and marine power systems. He is a member of scientific program committees of several IEEE conferences. He is also a Reviewer of several IEEE and IET journals, a Guest and an Associate Editor of several special issues in IEEE, IET, and Elsevier.